Acta Geotechnica (2009) 4:117–127
DOI 10.1007/s11440-008-0072-1

RESEARCH PAPER

A new algorithm to model the dynamics of 3-D bonded rigid bodies with rotations

Yucang Wang

Received: 28 June 2007 / Accepted: 6 May 2008 / Published online: 28 October 2008

Abstract In this paper we propose a new algorithm to simulate the dynamics of 3-D interacting rigid bodies. Six degrees of freedom are introduced to describe a single 3-D body or particle, and six relative motions and interactions are permitted between bonded bodies. We develop a new decomposition technique for 3-D rotation and pay particular attention to the fact that an arbitrary relative rotation between two coordinate systems or two rigid bodies can not be decomposed into three mutually independent rotations around three orthogonal axes. However, it can be decomposed into two rotations, one pure axial rotation around the line between the centers of two bodies, and another rotation on a specified plane controlled by another parameter. These two rotations, corresponding to the relative axial twisting and bending in our model, are sequence-independent. Therefore all interactions due to the relative translational and rotational motions between linked bodies can be uniquely determined using such a two-step decomposition technique. A complete algorithm for one such simulation is presented. Compared with existing methods, this algorithm is physically more reliable and has greater numerical accuracy.

Keywords Bonded rigid-bodies · Decomposition of 3-D finite rotations · Quaternion

List of symbols

Coordinate systems

$O-XYZ$	the space-fixed system
$O_1-X_1Y_1Z_1$	the body-fixed frame of particle 1
$O_2-X_2Y_2Z_2$	the body-fixed frame of particle 2
$O_2-X_2'Y_2'Z_2'$	an auxiliary body-fixed frame of particle 2, obtained by directly rotating $X_2Y_2Z_2$ at T = 0 such that its Z_2'-axis is pointing to particle 1. There is no relative rotation between $X_2'Y_2'Z_2'$ and $X_2Y_2Z_2$
$O_2-X_1'Y_1'Z_1'$	another auxiliary frame. The relative rotation from $X_2Y_2Z_2$ to $X_1Y_1Z_1$ makes $X_2'Y_2'Z_2'$ rotate to $X_1'Y_1'Z_1'$

Vectors

$\boldsymbol{f}$	total force acting on the particle, measured in the space-fixed system XYZ
$\boldsymbol{\tau}^b$	total torque acting on the particle expressed in body-fixed frame
$\boldsymbol{f_r}$	normal force between two particles
$\boldsymbol{f_{s1}}, \boldsymbol{f_{s2}}$	shear forces between two particles
$\boldsymbol{\tau_t}$	torque cause by twisting or torsion between two particles
$\boldsymbol{\tau_{b1}}, \boldsymbol{\tau_{b2}}$	torques cause by relative bending between two particles
$\Delta\boldsymbol{\alpha_t}$	relative angular displacement caused by twisting motion
$\Delta\boldsymbol{\alpha_{b1}}, \Delta\alpha_{b2}$	relative angular displacements caused by bending motion
$\Delta\boldsymbol{u_r}$	relative displacement in normal direction
$\Delta\boldsymbol{u_{s1}}, \Delta\boldsymbol{u_{s2}}$	relative displacements in tangent directions

Y. Wang (✉)
Earth Systems Science Computational Centre,
The University of Queensland, St Lucia,
Brisbane, QLD 4072, Australia
e-mail: wangyc@esscc.uq.edu.au; yucang_wang@hotmail.com

Y. Wang
Australian Computational Earth Systems Simulator (ACcESS),
MNRF, The University of Queensland,
St Lucia, Brisbane, QLD 4072, Australia

$\boldsymbol{r}$	position vector of a particle, measured in XYZ
$\boldsymbol{\omega}^b$	angular velocities measured in the body-fixed frame
$\boldsymbol{r}_{10}$, $\boldsymbol{r}_{20}$	initial position of particle 1 and particle 2, measured in XYZ
$\boldsymbol{r}_1$, $\boldsymbol{r}_2$	current positions of particle 1 and particle 2, measured in XYZ
$\boldsymbol{r}_0$	initial position of particle 1 relative to particle 2, measured in $X_2Y_2Z_2$ (or XYZ)
$\boldsymbol{r}_c$	current position of particle 1 relative to particle 2, measured in $X_2Y_2Z_2$
$\boldsymbol{r}_f$	current position of particle 1 relative to particle 2, measured in XYZ
$\Delta\boldsymbol{r}$	translational displacement of particle 1 relative to particle 2, measured in $X_2Y_2Z_2$
$\boldsymbol{f}_s^t$	shear force caused by translational motion of particle 1 relative to particle 2, measured in $X_2Y_2Z_2$
$\boldsymbol{\tau}_s^t$	torque generated by f_s^t, measured in $X_2Y_2Z_2$
$\boldsymbol{f}_s^r$	shear force caused by the rotation of particle 1 relative to particle 2, measured in $X_2Y_2Z_2$
$\boldsymbol{\tau}_s^r$	torque generated by f_s^r, measured in $X_2Y_2Z_2$
$\boldsymbol{\tau}_b^r$	bending torque cause by the rotation of particle 1 relative to particle 2, measured in $X_2Y_2Z_2$
$\boldsymbol{\tau}_t^r$	twisting torque cause by the rotation of particle 1 relative to particle 2, measured in $X_2Y_2Z_2$
$\boldsymbol{\tau}_b'$	bending torque cause by the rotation of particle 1 relative to particle 2, measured in $X_2'Y_2'Z_2'$
$\boldsymbol{\tau}_t'$	twisting torque cause by the rotation of particle 1 relative to particle 2, measured in $X_2'Y_2'Z_2'$
$\boldsymbol{f}_s'$	shear force caused by the rotation of particle 1 relative to particle 2, measured in $X_2'Y_2'Z_2'$
$\boldsymbol{\tau}_s'$	torque generated by f_s, measured in $X_2'Y_2'Z_2'$

Matrices

$\boldsymbol{\Omega}$	matrix of angular velocity
$\dot{\boldsymbol{Q}}$	matrix of quaternion derivative
$\boldsymbol{Q}_0$ (q)	matrix linking Ω and $\dot{Q}$

Quaternions

p^0, q^0	initial orientations of particle 1 and particle 2, expressed in XYZ
p, q	current orientations of particle 1 and particle 2, expressed in XYZ
g^o	rotation from $X_2Y_2Z_2$ to $X_1Y_1Z_1$, expressed in $X_2Y_2Z_2$
g	rotation from $X_2'Y_2'Z_2'$ to $X_1'Y_1'Z_1'$, expressed in $X_2'Y_2'Z_2'$
h	rotation from $X_2Y_2Z_2$ to $X_2'Y_2'Z_2'$, expressed in $X_2Y_2Z_2$

Others

ψ	twisting angle between two particles
θ	bending angle between two particles
φ	orientation angle determining the plane on which bending occurs
K_r	normal stiffness
K_s, K_{s1}, K_{s2}	shear stiffness
K_t	twisting (torsional) stiffness
K_b K_{b1}, K_{b2}	bending stiffness
M	mass of a rigid body or particle
I_{xx}, I_{yy}, I_{zz}	three principle moments of inertia in the body-fixed frame

1 Introduction

There is growing interest in simulating the dynamics of 3-D interacting rigid bodies in many fields. For example, the field of molecular dynamics (MD) sometimes models systems of classical rigid molecules [1, 25]; particle-based models, such as the discrete element method [6, 24] and the lattice solid model [18], typically consider an assemblage of rigid particles linked by springs. Similar applications can also be found in chemical physics [2] and bio-physics [5, 17].

In such studies, it is crucial to consider three important factors: the representation of the degree of freedoms for each rigid body, integration of the equations of motions and calculation of the interactions (e.g. forces and torques) between bonded bodies. Theoretically, six degrees of freedom (DOF) are required to completely describe a single 3-D rigid body. Therefore six independent relative movements and six interactions are permitted between two interacting rigid bodies. In certain cases it is a good approximation to use a simple model where rotation is not permitted. However, there exist plenty of examples where it is necessary to consider not only the stretching of bonds, but also the bending and twisting of bonds. Nearly 20 years ago these effects were thought to be rather unrealistic and were not properly accounted for within a classical framework [1]. The reason is that if the rotation of a single rigid body is involved and six interactions are permitted, the factors discussed above, especially the third one, become more complicated than the simple model.

There are numerous investigations concerning the first two problems. For example, it is found that performing a

straightforward parameterization of the orientational degrees of freedom of a 3-D rigid body, using a Euler angle representation, is not numerically efficient because of a singularity inherent in this description [8, 9]. To avoid this singularity, orientations are typically expressed in terms of a unit quaternion [8, 9, 14, 21], rotation matrices [15, 22] and vectors [3, 4, 19].

Different numerical algorithms are employed to discover the optimal approach to integrate the rotational equations, such as high-order Gear methods [1], leapfrog-like algorithms [10] and more recently symplectic splitting method [15]. However, previous studies have not addressed the third equally important issue which is the calculation of interactions (or potential) between bonded bodies caused by the relative rotation between bodies. In the 2-D case, it is quite easy to calculate sliding and rolling distances [12, 13]. However, in 3-D it becomes more complicated because of the non-commutative nature of finite rotation.

To our knowledge, there are very few 3-D models involving full rigidity between bonded rigid bodies. One such model we know is the Discrete Element Model [24]. In this model, the incremental method is used to calculate interactions caused by relative rotations and tangential motion between bonded particles. However, the incremental method does not provide an ideal solution. As we reveal later, it is not as stable and accurate as the method proposed in this paper because it is only physically correct in the infinitesimal limit.

An alternate way to solve the problem is to decompose the relative rotations between two rigid bodies into several independent angular displacements such that the torques and forces can be determined. The conventional method widely employed is to factorize the rotation into three successive rotations (Euler/Cardan angles). Unfortunately, such sequential rotations are sequence-dependent and mutually independent. For this reason, the torques and forces can not be determined uniquely.

In this paper, we formulate a physical and order-independent decomposition of a 3-D rotation which is correct for any finite rotation and leads to a numerically stable scheme. A complete scheme for the 3-D motion of interactive multi-bodies with six DOF is provided. This paper is arranged as follows: in Sect. 2 our model with six DOF is described. The equations of motion and detailed algorithms for solving the rotational equations are given in Sect. 3. Section 4 gives expressions for interactions caused by the relative translational motions between two particles. A new way of decomposing a finite rotation is presented in the Appendix. Comparisons between our new algorithm and existing algorithms are presented in Sect. 5, and also we present some numerical examples in this section to test our model and algorithm and finally we present our conclusions and discussions of results in Sect. 6.

2 Model of six relative motions with six degrees of freedom

To completely describe a 3-D rigid body, one needs six degrees of freedom, three for the center position of the rigid body, and three for the rotations around the center of the mass. Any arbitrary relative movement between two bodies can be considered as a combination of six independent relative motions: tension or compression along the radial direction, shown in Fig. 1a, two shearing motions along the tangential direction (Fig. 1b), twisting (Fig. 1c) and two bending motions (Fig. 1d). Note that in the case of pure bending (Fig. 1d), there is no relative sliding at the contact point. The six relative motions are also known as rise, shift, slide, tilt, roll and twist in bio-mechanics literature [5].

Under the assumption of small deformation, relationships between the interactions (forces or torques) and relative displacements can be written as the following linear forms

$$\begin{aligned} \boldsymbol{f}_r &= K_r \Delta \boldsymbol{u}_r,\ \boldsymbol{f}_{s1} = K_{s1} \Delta \boldsymbol{u}_{s1},\ \boldsymbol{f}_{s2} = K_{s2} \Delta \boldsymbol{u}_{s2}, \boldsymbol{\tau}_t \\ &= K_t \Delta \boldsymbol{\alpha}_t, \boldsymbol{\tau}_{b1} = K_{b1} \Delta \boldsymbol{\alpha}_{b1}, \boldsymbol{\tau}_{b2} = K_{b2} \Delta \boldsymbol{\alpha}_{b2} \end{aligned} \quad (1)$$

where $\Delta \boldsymbol{u}_r$, $\Delta \boldsymbol{u}_{s1}$ ($\Delta \boldsymbol{u}_{s2}$) are the relative displacements in normal and tangent directions. $\Delta \boldsymbol{\alpha}_t$ and $\Delta \boldsymbol{\alpha}_{b1}(\Delta \boldsymbol{\alpha}_{b2})$ are the relative angular displacements caused by twisting and bending. $\boldsymbol{f}_r, \boldsymbol{f}_{s1}, \boldsymbol{f}_{s2}, \boldsymbol{\tau}_t, \boldsymbol{\tau}_{b1}$ and $\boldsymbol{\tau}_{b2}$ are forces and torques, K_r, K_{s1}, K_{s2}, K_t, K_{b1} and K_{b2} are relevant stiffness. Here subscripts r, s, t and b stand for radial (normal), shearing, twisting and bending. In the isotropic case, $K_s = K_{s1} = K_{s2}$ and $K_b = K_{b1} = K_{b2}$.

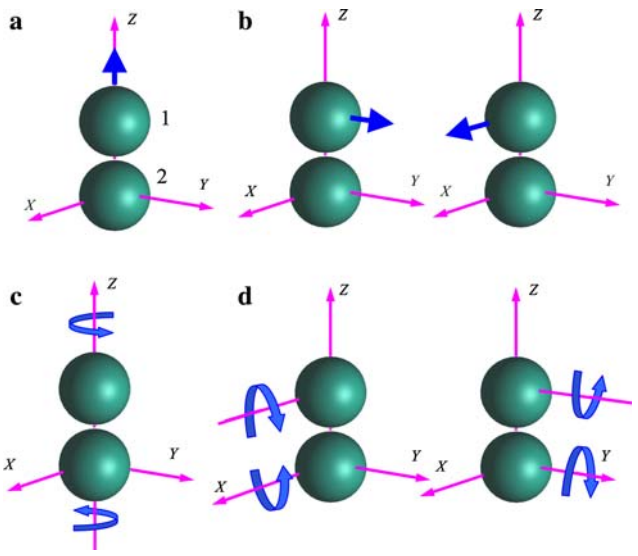

Fig. 1 Six interactions between bonded particels. **a** Pulling or pressing in radial direction. **b** Shearing in two tangential directions, **c** twisting, **d** bending

3 Representation of rotation and the equations of motion

Rigid-body motion can be decomposed into two completely independent parts, translational motion of the center of mass and rotation about the center. The former is governed by the Newtonian equation

$$\ddot{\boldsymbol{r}}(t) = \boldsymbol{f}(t)/M \tag{2}$$

where $\boldsymbol{r}(t), \boldsymbol{f}(t)$ and M are the position vector of the particle, the total forces acting on the particle and the particle mass respectively. A conventional molecular scheme can be used to integrate the equation above [1, 18, 23].

The rigid body rotation depends on the total applied torque and usually involves two coordinate frames, one is fixed in space, referred to as a space-fixed frame, and the other is attached to the principal axes of the rotation body, referred to as a body-fixed frame. In the body-fixed frame, the dynamic equations are [11]

$$\begin{aligned}
\tau_x^b &= I_{xx}\dot{\omega}_x^b - \omega_y^b\omega_z^b(I_{yy} - I_{zz}),\\
\tau_y^b &= I_{yy}\dot{\omega}_y^b - \omega_z^b\omega_x^b(I_{zz} - I_{xx}),\\
\tau_z^b &= I_{zz}\dot{\omega}_z^b - \omega_x^b\omega_y^b(I_{xx} - I_{yy})
\end{aligned} \tag{3}$$

Where τ_x^b, τ_y^b and τ_z^b are components of the total torque $\boldsymbol{\tau}^b$ expressed in body-fixed frame, ω_x^b, ω_y^b and ω_z^b are components of the angular velocities $\boldsymbol{\omega}^b$ measured in the body-fixed frame, and I_{xx}, I_{yy} and I_{zz} are the three principle moments of inertia in the body-fixed frame in which the inertia tensor is diagonal. In the case of a three-dimensional sphere, $I = I_{xx} = I_{yy} = I_{zz}$.

Due to the singularity caused by Euler angles, the unit quaternion $q = q_0 + q_1 i + q_2 j + q_3 k$ is usually employed to describe orientations in numerical simulations [8, 9], where $\sum_{i=0}^{3} q_i^2 = 1, i^2 = j^2 = k^2 = ijk = -1, ij = -ji = k$, $jk = -kj = i$, and $ki = -ik = j$. The physical meaning of a quaternion is that it represents a one-step rotation through the angle of 2arc cos(q_0) about the vector $q_1\hat{i} + q_2\hat{j} + q_3\hat{k}$ [16]. This is a very convenient tool since sequences of rotations can be conveniently represented as quaternion product [16].

The quaternion for each particle satisfies the following equations [8, 9]

$$\dot{\boldsymbol{Q}} = \frac{1}{2}\boldsymbol{Q_0}(q)\Omega \tag{4}$$

where $\dot{\boldsymbol{Q}} = \begin{pmatrix} \dot{q}_0 \\ \dot{q}_1 \\ \dot{q}_2 \\ \dot{q}_3 \end{pmatrix}$, $Q_0(q) = \begin{pmatrix} q_0 & -q_1 & -q_2 & -q_3 \\ q_1 & q_0 & -q_3 & q_2 \\ q_2 & q_3 & q_0 & -q_1 \\ q_3 & -q_2 & q_1 & q_0 \end{pmatrix}$,

$\Omega = \begin{pmatrix} 0 \\ \boldsymbol{\omega}_x^b \\ \boldsymbol{\omega}_y^b \\ \boldsymbol{\omega}_z^b \end{pmatrix}$.

There are different ways to solve Eqs. 3 and 4 numerically. The most simplest and widely used one is the explicit leapfrog algorithm [1, 10], which is reported to be stable and accurate with a moderate time step [1]. It is outlined below for the completeness of this paper.

We can obtain the quaternion $q(t + \Delta t)$ at the next time step using:

$$\begin{aligned}
q(t + \Delta t) &= q(t) + \Delta t\dot{q}(t) + \frac{\Delta t^2}{2}\ddot{q}(t) + O(\Delta t^3)\\
&= q(t) + \Delta t\dot{q}(t + \Delta t/2) + O(\Delta t^3)
\end{aligned} \tag{5}$$

Hence, the quaternion derivative at mid-step ($\dot{q}(t + \Delta t/2)$) is required. Eq. 4 indicates that $q(t + \Delta t/2)$ and $\boldsymbol{\omega}^b(t + \Delta t/2)$ are also required, where the former can be easily calculated using

$$q(t + \Delta t/2) = q(t) + \dot{q}(t)\Delta t/2 \tag{6}$$

where $\dot{q}(t)$ again is given by Eq. 4, and $\boldsymbol{\omega}^b(t)$ can be calculated using

$$\boldsymbol{\omega}^b(t) = \boldsymbol{\omega}^b(t - \Delta t/2) + I^{-1}\boldsymbol{\tau}^b(t)\Delta t/2 \tag{7}$$

and $\boldsymbol{\omega}^b(t + \Delta t/2)$ can be obtained using

$$\boldsymbol{\omega}^b(t + \Delta t/2) = \boldsymbol{\omega}^b(t - \Delta t/2) + I^{-1}\boldsymbol{\tau}^b(t)\Delta t \tag{8}$$

In this algorithm, only $\boldsymbol{\omega}^b(t - \Delta t/2)$ and $q(t)$ need to be stored, whereas the other quantities, such as $q(t + \Delta t/2), \boldsymbol{\omega}^b(t), \dot{q}(t), \dot{q}(t + \Delta t/2)$ etc are treated as temporary and auxiliary values.

To avoid build-up errors, it is a common practice to renormalize the quaternions at frequent intervals (usually done at every time-step). The whole algorithm proceeds as follows:

Step 1: calculate the force $\boldsymbol{f}$ and torque $\boldsymbol{\tau}^b(t)$ according to Eqs. 12–19.
Step 2: update $\boldsymbol{\omega}^b(t)$ using the stored $\boldsymbol{\omega}^b(t - \Delta t/2)$ according to Eq. 7.
Step 3: obtain $\dot{q}(t)$ using Eq. 4.
Step 4: calculate $\omega^b(t + \Delta t/2)$ using the stored $\omega^b(t - \Delta t/2)$ according to Eq. 8.
Step 5: compute $q(t + \Delta t/2)$ using Eq. 6.
Step 6: evaluate $\dot{q}(t + \Delta t/2)$ using Eq. 4.
Step 7: calculate $q(t + \Delta t)$ using Eq. 5.
Step 8: renormalize the quaternion $q(t + \Delta t)$.

In recently years, more advanced and accurate algorithms have been proposed which focus on conserving the symplectic structure, time reversible and energy [4, 7, 15, 20, 21].

4 Calculation of forces and torques between two rigid bodies due to their relative motion

Before solving Eqs. 2–4, one important problem remains: given the position and orientation for each particle, how

can one calculate the forces and torques between bonded particles due to their relative motion? This requires decomposition of the relative motions and is the crucial step for obtaining reliable and accurate results.

Suppose that in the space-fixed frame, the initial positions of particle 1 and 2 at time $T = 0$ are $\boldsymbol{r}_{10} = x_{10}\boldsymbol{i} + y_{10}\boldsymbol{j} + z_{10}\boldsymbol{k}$ and $\boldsymbol{r}_{20} = x_{20}\boldsymbol{i} + y_{20}\boldsymbol{j} + z_{20}\boldsymbol{k}$ (Fig. 2), and their initial orientations are $p^0 = 1 + 0i + 0j + 0k$ and $q^0 = 1 + 0i + 0j + 0k$. At time t, the current positions $\boldsymbol{r}_1 = x_1\boldsymbol{i} + y_1\boldsymbol{j} + z_1\boldsymbol{k}$ and $\boldsymbol{r_2} = x_2\boldsymbol{i} + y_2\boldsymbol{j} + z_2\boldsymbol{k}$ and current orientations $p = p_0 + p_1 i + p_2 j + p_3 k$ and $q = q_0 + q_1 i + q_2 j + q_3 k$, are known for particle 1 and 2. To calculate the interactions between these two particles, the relative motion between the two particles needs to be determined first. Our original goal is to decompose this relative motion into six independent motions as shown in Fig. 1. The key idea is to consider the overall motion of particle 1 relative to particle 2 during the interval from $T = 0$ to t. Taking particle 2 as a reference, we can decompose the relative motion of particle 1 into two independent parts: its relative translational motion and relative rotation.

Let $O_2 - X_2Y_2Z_2$ (later referred as $X_2Y_2Z_2$) and $O_1 - X_1Y_1Z_1$ represent the body-fixed frame of particle 2 and 1 respectively. The relative translational displacement of particle 1 with respect to $X_2Y_2Z_2$ (Fig. 3) is

$$\Delta \boldsymbol{r} = \boldsymbol{r_c} - \boldsymbol{r_0} \tag{9}$$

where

$$\boldsymbol{r}_0 = \boldsymbol{r}_{10} - \boldsymbol{r_{20}} = x_{12}\boldsymbol{i} + y_{12}\boldsymbol{j} + z_{12}\boldsymbol{k} \tag{10}$$

is the initial position (at which the force between two particles is zero) of particle 1 relative to particle 2, measured in XYZ (Fig. 2) or $X_2Y_2Z_2$ (Fig. 3, since the initial orientation of $X_2Y_2Z_2$ is the same with XYZ) and $\boldsymbol{r_c}$ is the current position of particle 1 relative to particle 2, measured in $X_2Y_2Z_2$, and

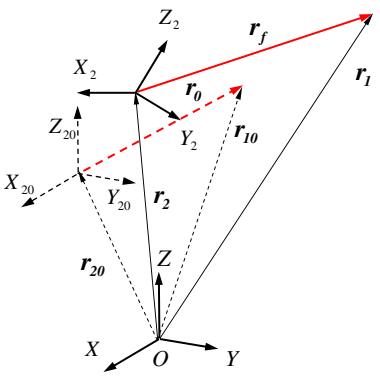

Fig. 2 Absolute positions of particle 1 and 2 at $T = 0$ and $T = t$, evaluated in space-fixed frame. $X_{20}Y_{20}Z_{20}$ here represents the body-fixed frame of particle 2 at $T = 0$

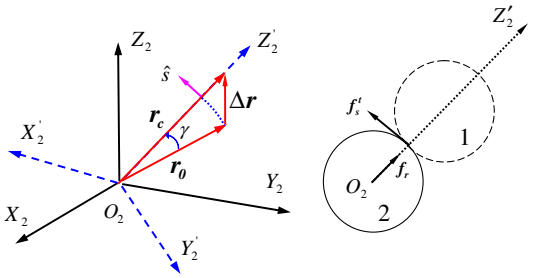

Fig. 3 The relative translational displacements of particle 1 relative to particle 2 with respect to $X_2Y_2Z_2$ co-ordinates is $\Delta \mathbf{r}.\mathbf{r}_0$ and $\mathbf{r}_c$ are initial and current relative position of particle 1 in $X_2Y_2Z_2$. The right plot describes the direction of the forces exerted on particle 2

$$\boldsymbol{r_c} = q^{-1}\boldsymbol{r_f}q \tag{11}$$

where $\boldsymbol{r_f} = \boldsymbol{r_1} - \boldsymbol{r_2}$ is the current position of particle 1 relative to particle 2, measured in the space-fixed system $O{-}XYZ$ (Fig. 2). In Eq. 11 the possible motion and rotation of particle 2 have been taken into account. In case of $|\Delta \boldsymbol{r}| \ll |\boldsymbol{r_c}|$ and $|\Delta \boldsymbol{r}| \ll |\boldsymbol{r_0}|$, the normal force acting on particle 2 becomes

$$\boldsymbol{f_r} = K_r(|\boldsymbol{r_c}| - |\boldsymbol{r}_0|)\boldsymbol{r_c}/|\boldsymbol{r_c}| \tag{12}$$

The shearing force acting on particle 2 has two contributions

$$\boldsymbol{f_s} = \boldsymbol{f_s^t} + \boldsymbol{f_s^r} \tag{13}$$

where

$$\boldsymbol{f_s^t} = K_s|\boldsymbol{r_0}|\gamma\hat{\boldsymbol{s}} \tag{14}$$

is caused by the translational shear displacement ($|\boldsymbol{r_0}|\gamma$) of particle 1 relative to $X_2Y_2Z_2$ without relative rotation. The angle γ is determined by $\cos\gamma = \boldsymbol{r_0}\cdot\boldsymbol{r_c}/|\boldsymbol{r_0}||\boldsymbol{r_c}|$ and the direction of $\boldsymbol{f_s^t}$ is determined by unit vector $\hat{\boldsymbol{s}} = \boldsymbol{r_c} \times (\boldsymbol{r_c} \times \boldsymbol{r_0})/|\boldsymbol{r_c} \times (\boldsymbol{r_c} \times \boldsymbol{r_0})|$.

Since $\boldsymbol{f_s^t}$ is exerted on the contact surface of the rigid bodies (or exerted in the geometric center of the two body system), rather than the center of particle 2, it generates a torque

$$\boldsymbol{\tau_s^t} = \frac{1}{2}|\boldsymbol{r_c}||\boldsymbol{f_s^t}|\hat{\boldsymbol{t}} \tag{15}$$

where the unit vector $\hat{\boldsymbol{t}} = \boldsymbol{r_0} \times \boldsymbol{r_c}/|\boldsymbol{r_0} \times \boldsymbol{r_c}|$ specifies the direction of $\boldsymbol{\tau_s^t}$. Note that Eqs. 12, 14 and 15 are evaluated in $X_2Y_2Z_2$ co-ordinates.

$\boldsymbol{f_s^r}$ in Eq. 13, which is caused by the relative rotation of particle 1 with respect to $X_2Y_2Z_2$, is calculated using our rotation decomposition technique (detailed in the Appendix).The main concepts are highlighted below.

The relative rotation from $X_2Y_2Z_2$ to $X_1Y_1Z_1$ is represented by the quaternion $g^o = q^{-1}p = q^*p$, where $q^{-1} = q^* = q_0 - q_1 i - q_2 j - q_3 k$. Let $O_2 - X_2'Y_2'Z_2'$ be an auxiliary body-fixed frame of particle 2, obtained by

directly rotating $X_2Y_2Z_2$ such that its Z_2'-axis is pointing to the particle 1 at time $T = 0$ (Fig. 3). $X_2'Y_2'Z_2'$ is fixed in $X_2Y_2Z_2$ and there is no relative rotation between $X_2'Y_2'Z_2'$ and $X_2Y_2Z_2$. It is the $X_2'Y_2'Z_2'$ system in which the relative rotation between the two particles should be evaluated (Fig. 1). Such relative rotation corresponds to the rotation from $X_2'Y_2'Z_2'$ to another auxiliary frame $O_2 - X_1'Y_1'Z_1'$ (Figs. 4, 8, 9. Only the Z_1'-axis is drawn in Fig. 4), and can be decided by the quaternion $g = h^{-1}g^o h = g_0 + g_1 i + g_2 j + g_3 k$ (expressed in $X_2'Y_2'Z_2'$ system), where the quaternion h specifies the rotation from $X_2Y_2Z_2$ to $X_2'Y_2'Z_2'$ (Eq. 20 in Appendix).

Using quaternion algebra, we proved (see Appendix) that the rotation from $X_2'Y_2'Z_2'$ to $X_1'Y_1'Z_1'$ can not be decomposed into three mutually independent rotations around three principal axes. However it can be decomposed into two rotations, one rotation of Z_2'-axis over θ on a specified plane controlled by parameter φ and another rotation of angle ψ about the new Z_2'-axis (Z_1'-axis) (Fig. 4). The two rotations, corresponding to the bending and twisting between two bodies in our model, are sequence-independent. As will be demonstrated in Figs. 8 and 9 later, this means that we can either start from a rotation of angle θ from Z_2'-axis to Z_1'-axis first, then followed by an axial rotation of angle ψ about Z_1'-axis (Figs. 8, 4, corresponds to this), or change orders of the two rotations such that an axial rotation of angle ψ' about Z_2'-axis is followed by a rotation of angle θ from the Z_2' -axis to the Z_1'-axis (Fig. 9).

The beauty of this sequence-independent decomposition is that it respects the physical law and it is guaranteed that forces and torques decided by such a two-step rotation are unique. The parameters ψ, θ and φ are determined by Eqs. 24–26 (see Appendix).

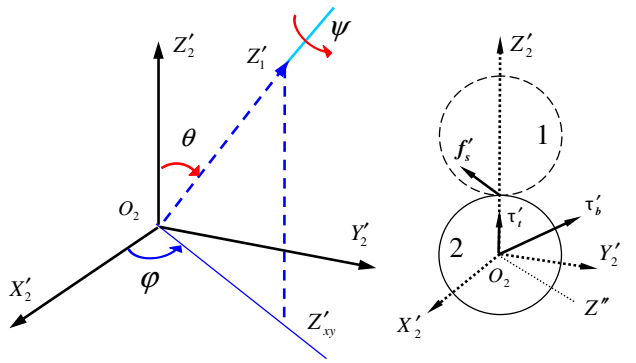

Fig. 4 Besides the angles θ and ψ, which specify pure bending and pure axial twisting, φ controls the orientation of the $Z_2'O_2Z_1'$ plane on which bending takes place, and can be regarded as the third rotational degree of freedom. The right plot describes the direction of the forces and torques exerted on particle 2 due to the relative rotation between the two particles

After applying this decomposition, the bending, twisting torque and shear forces exerted on particle 2 are (expressed in $X_2'Y_2'Z_2'$ co-ordinates)

$$\begin{aligned}
\boldsymbol{\tau}_b' &= K_b\theta(-\sin\varphi\hat{\boldsymbol{i}} + \cos\varphi\hat{\boldsymbol{j}}),\\
\boldsymbol{\tau}_t' &= K_t\psi\hat{\boldsymbol{k}},\\
\boldsymbol{f}_s' &= -K_s\frac{|\boldsymbol{r_0}|\theta}{2}(\cos\varphi\hat{\boldsymbol{i}} + \sin\varphi\hat{\boldsymbol{j}}),\\
\boldsymbol{\tau}_s' &= K_s\frac{|\boldsymbol{r_0}|^2\theta}{4}(\sin\varphi\hat{\boldsymbol{i}} - \cos\varphi\hat{\boldsymbol{j}})
\end{aligned} \tag{16}$$

where $\boldsymbol{\tau}_s'$ is the torque generated by $\boldsymbol{f}_s'$. It should be pointed out that Eqs. 15 and 16 are based on the assumption of two equally-sized spheres. For rigid bodies with different sizes and shapes, Eqs. 15 and 16 should be changed accordingly.

Torques and forces can be transformed from $X_2'Y_2'Z_2'$ to the $X_2Y_2Z_2$ frame

$$\boldsymbol{\tau}_b^r = h\boldsymbol{\tau}_b'h^{-1}, \quad \boldsymbol{\tau}_t^r = h\boldsymbol{\tau}_t'h^{-1}, \quad \boldsymbol{f}_s^r = h\boldsymbol{f}_s'h^{-1}, \quad \boldsymbol{\tau}_s^r = h\boldsymbol{\tau}_s'h^{-1} \tag{17}$$

The total forces and torques on each particle are expressed as the sum of contributions from all particles bonded to it

$$\boldsymbol{f} = \sum q(\boldsymbol{f}_r + \boldsymbol{f}_s^t + \boldsymbol{f}_s^r)q^{-1} \tag{18}$$

$$\boldsymbol{\tau}^b = \sum(\boldsymbol{\tau}_s^t + \boldsymbol{\tau}_s^r + \boldsymbol{\tau}_b^r + \boldsymbol{\tau}_t^r) \tag{19}$$

Since $\boldsymbol{f}$ in Eq. 2 is expressed in the space-fixed frame, but $\boldsymbol{f}_r$, $\boldsymbol{f}_s^t$ and $\boldsymbol{f}_s^r$ in Eqs. 12, 14 and 17 are all evaluated in the body-fixed frame, one more transfer (from the body-fixed to the space-fixed frame) is required in Eq. 18. Note that no more rotation is needed in Eq. 19 because $\boldsymbol{\tau}^b$ in Eq. 3 is expressed in the body-fixed frame and $\boldsymbol{\tau}_s^t$, $\boldsymbol{\tau}_s^r$, $\boldsymbol{\tau}_b^r$ and $\boldsymbol{\tau}_t^r$ are already expressed in the body-fixed frame (see Eqs. 15 and 17). Once forces and torques are obtained, Eqs. 2–4 can be integrated for each particle.

5 Numerical validations and comparisons between the algorithm described and existing algorithms

To test the novel algorithm described above, we performed simulations using a simple model. The model consists of seven bonded cubes (in order to visualize rotation). Six interactions are transferred between the neighboring cubes in the way shown in Fig. 1. The initial state is the system's natural state without any interactions (Fig. 5a). Slow constant velocities or angular velocities are exerted on the first and the last cube to make the whole chain deform. Figure 5b–f show the deformation of the chain after 40,000 time steps under compressing, shearing, bending, twisting and bending plus twisting conditions respectively. The continuous and uniform movements of all cubes in these simple tests indicate that all interactions were transferred

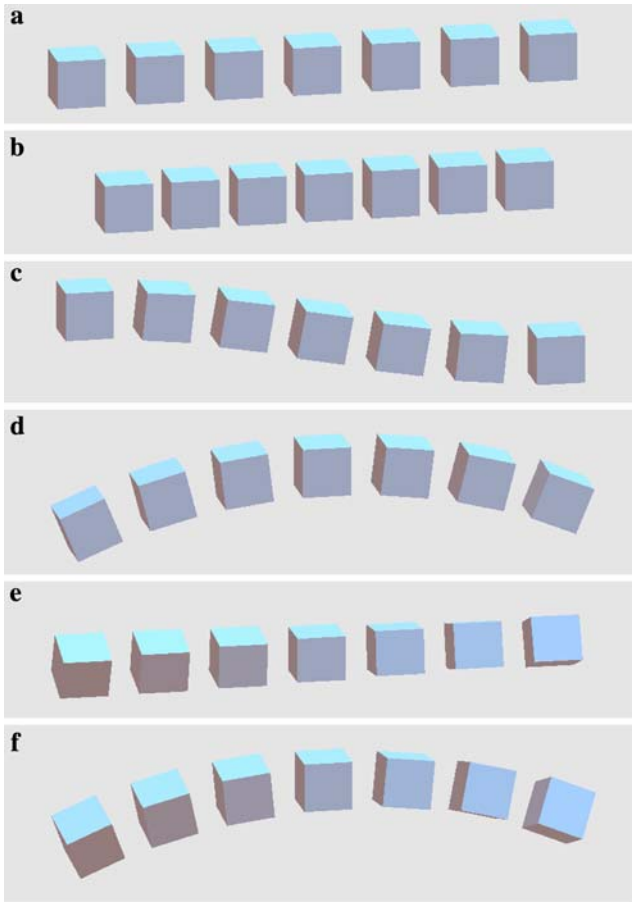

Fig. 5 Deformation of the chain after 40,000 time steps under boundary conditions of compressing (**b**), shearing (**c**), pure bending (**d**), pure twisting (**e**) and bending plus twisting loading (**f**)

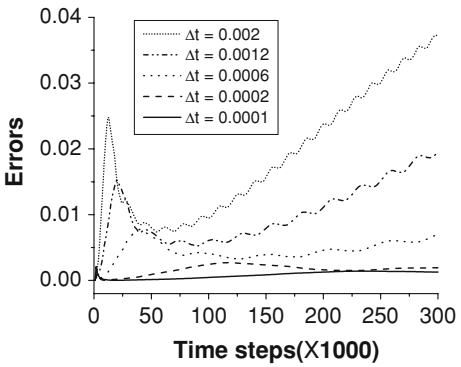

Fig. 6 Evolution of relative errors with time in the incremental method for different time step sizes Δt (from 0.0001 to 0.002). The relative error is defined as (kinetic energy + potential energy – external work)/(external work). The errors increase much faster with increasing time step size Δt

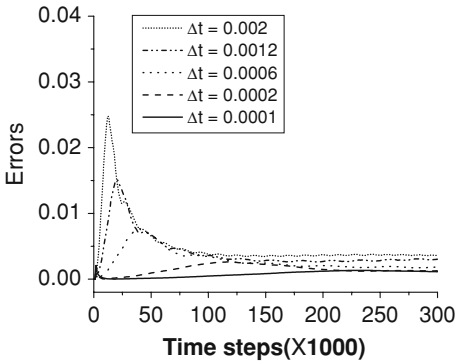

Fig. 7 Evolution of relative errors in our algorithm for different time step sizes Δt. In our algorithm, the errors do not increase too much with increasing time step size Δt

properly, which provides validation of our model and algorithm.

Figures 6 and 7 compare the relative errors incurred using the incremental method and using our algorithm for different time step sizes Δt (in the case of bending and twisting of the simple model, Fig. 5f). The relative error is defined as (kinetic energy + potential energy−external work)/(external work). We have found that the errors produced by the incremental method increase much faster than those in our algorithm when the time step is increasing, indicating that our algorithm is more accurate and stable over a greater range of time step sizes.

We also implemented our algorithm into a much more complex 3-D particle based model, the Lattice Solid Model. Several tests using 2-D and 3-D rock failure were carried out [26, 27]. Compared with simulations where only radial interactions were transmitted between bonded particles, the new simulation results match more closely with that of experimental results of rock fracture. This provides further support for our algorithm.

Our algorithms to calculate the forces and torques due to relative rotations in Sect. 4 are unique and advantageous over existing algorithms [24] in the following aspects: firstly we make use of a quaternion to represent the orientation of a rigid body. Currently there are no *explicit* rotational degrees of freedom for rigid bodies in most existing models. By *explicit*, we mean that once the explicit variable is given, the orientation of a 3-D particle is uniquely determined. Candidates of such variables include matrix, quaternion, vector, Euler Angles. In the most models orientations are *implicitly* represented using three angular velocities around three orthogonal axes. In the 2-D case this does not present a problem, since an angle can be easily integrated from angular velocities for each rigid body at each time step, thereby defining the orientation. However, in the 3-D case, one can not extract the exact orientation of each rigid body by simply integrating with the three angular velocities. The reason is that even if the three angles are obtained by integration, the exact orientation of a rigid body still can not be uniquely decided,

since *finite rotations in 3-D are order dependent*! In other words, for the same three finite angles, different sequences of rotations will result in different final orientations. This salient feature of finite rotations in 3-D is one which is ignored by most modelers, and in this paper we attempt to address and highlight this discrepancy.

Secondly, our algorithm is based on the method (we term finite deformation method) in which total displacements are calculated instead of incremental displacements (Eq. 1). At each time step t, we only need the initial and current position and orientation (i.e. at $T = 0$ and t). In nearly all other algorithms, shear forces and torques are computed in an incremental fashion [24]. This means that the three incremental angles from time $t - \Delta t$ to t are computed using three angular velocities, then the three incremental torques are calculated and added to the torques at time $t - \Delta t$ to get the torques at time t. It should be noted that when twisting and bending co-exist, bending changes the axis of twisting, and thus, the incremental method fails to decouple the twisting and bending. Using our decomposition technique, twisting and bending are completely decoupled, strictly distinguished and sequence-independent. Therefore our algorithm is physically reliable. It is extremely useful to apply our method when twisting and bending stiffnesses are different.

Lastly, from a theoretical standpoint, only infinitesimal rotations in 3-D are order independent. Hence, in order to gain accurate results, the incremental method requires very small time steps. This computational inefficiency is highlighted in Fig. 6, where the errors in the incremental method are shown to increase much faster than those in our algorithm with increasing time step.

6 Discussions and conclusions

We developed a new algorithm for modeling 3-D motions of bonded rigid bodies. In the new model, six parameters are introduced to describe a single rigid body and each rigid body is permitted to rotate. Neighboring bodies can be bonded together by springs through which six interactions can be transmitted. The crux of this algorithm is the decomposition of finite rotations. Our fundamental advancement to this method is that the relative rotation between two rigid bodies or two coordinate systems can be decomposed into two sequence-independent rotations, corresponding to twisting and bending on a specified plane. However, this relative rotation can not be decomposed into three mutually independent rotations, since the bending can not be further geometrically separated into two independent bending motions around two orthogonal axes. Fortunately, in the isotropic case, such a decomposition is not necessary, since interactions due to the relative rotations can still be calculated using a twisting angle ψ, a bending angle θ and the third parameter φ which determines the plane on which bending occurs.

We outlined earlier the core differences between our algorithm and most current algorithms. The pivotal advantages of our algorithm over the incremental method include the existence of a rotational degree of freedom for each single body, the existence of distinguishable and decoupled twisting and bending motions, the larger time steps permitted and the physical principles taken into account. Our algorithm is physically clear, reliable and numerically more accurate.

Since our goal is to demonstrate the reliability and advantages of our new decomposition technique for 3-D rotation, we have mainly focused on the calculation of forces and torques between linked bodies. For this reason we do not compare any algorithms for integrating the rotational equations adopted in this paper with more recent ones proposed by [7, 15, 20–22], which are reported to be more accurate and stable. This comparison will pave the way for future work.

Our initial intention is to apply this algorithm to our Discrete Element Model [18, 23, 26]. However, the scheme presented in this paper has widespread applicability and appeal and may also be applied to advance the current state of modeling in many other fields including molecular dynamics, chemical physics, bio-physics and other simulations.

Acknowledgments Funding support is gratefully acknowledged by the Australian Computational Earth Systems Simulator Major National Research Facility, The University of Queensland and SGI. The ACcESS MNRF is funded by the Australian Commonwealth Government and participating institutions (University of Queensland, Monash U, Melbourne U., VPAC, RMIT) and the Victorian State Government. The author would like to thank Dr. Louise Kettle, Mr. William Hancock and Dr. Junfang Zhang for their valuable suggestions to improve the manuscript.

Appendix: Decomposition of finite rotations and calculation of interactions due to relative rotations

Decomposition of the relative translational motions is discussed in Sect. 4. In this part we focus on the decomposition of the relative rotations. This decomposition provides a mathematical basis for our algorithm.

As shown in Sect. 4, the relative rotation of particle 1 over particle 2, or rotation from $X_2Y_2Z_2$ to $X_1Y_1Z_1$, is represented by a quaternion $g^o = q^{-1}p = q^*p$. We choose to evaluate the relative motion between the two particles in $X_2'Y_2'Z_2'$ co-ordinate (Fig. 3). The relative rotation g^o

corresponds to the rotation from $X_2'Y_2'Z_2'$ to $X_1'Y_1'Z_1'$, which is determined by the quaternion $g = h^{-1}g^o h = g_0 + g_1 i + g_2 j + g_3 k$ (expressed in the $X_2'Y_2'Z_2'$ co-ordinate system), where the quaternion $h = h_0 + h_1 i + h_2 j + h_3 k$ specifies the rotation from $X_2Y_2Z_2$ to $X_2'Y_2'Z_2'$. The axis and angle of this rotation is determined by the vector $\hat{\boldsymbol{k}} \times \boldsymbol{r_c} = -y_{12}\hat{\boldsymbol{i}} + x_{12}\hat{\boldsymbol{j}}$ (evaluated in $X_2Y_2Z_2$) and the angle θ', where $\cos\theta' = z_{12}\Big/\sqrt{x_{12}^2 + y_{12}^2 + z_{12}^2}$. Considering that $h_0 = \cos(\theta'/2)$, $\sum_{i=0}^{3} h_i^2 = 1$ and $h_1\hat{\boldsymbol{i}} + h_2\hat{\boldsymbol{j}} + h_3\hat{\boldsymbol{k}} \propto \hat{\boldsymbol{k}} \times \boldsymbol{r_c}$, we have

$$
\begin{aligned}
h_0 &= \frac{\sqrt{2}}{2}\sqrt{\frac{\sqrt{x_{12}^2 + y_{12}^2 + z_{12}^2} + z_{12}}{\sqrt{x_{12}^2 + y_{12}^2 + z_{12}^2}}},\\
h_1 &= -\frac{\sqrt{2}}{2}\sqrt{\frac{\sqrt{x_{12}^2 + y_{12}^2 + z_{12}^2} - z_{12}}{\sqrt{x_{12}^2 + y_{12}^2 + z_{12}^2}}}\frac{y_{12}}{\sqrt{x_{12}^2 + y_{12}^2}},\\
h_2 &= \frac{\sqrt{2}}{2}\sqrt{\frac{\sqrt{x_{12}^2 + y_{12}^2 + z_{12}^2} - z_{12}}{\sqrt{x_{12}^2 + y_{12}^2 + z_{12}^2}}}\frac{x_{12}}{\sqrt{x_{12}^2 + y_{12}^2}},\\
h_3 &= 0
\end{aligned}
\tag{20}
$$

Our next goal is to decompose the rotation g into several rotations. As a first guess, we can factorize the quaternion g into three rotations around the three axes, such as XYZ-type successive rotations. These start with a rotation of β_1 about the X_2'-axis, followed by a rotation of β_2 about the new Y_2'-axis, and then finally a rotation of β_3 about the new Z_2'-axis. The quaternions of the three successive rotations are:

$$
\begin{aligned}
l_x &= \cos\frac{\beta_1}{2} + \sin\frac{\beta_1}{2}i, \quad l_y = \cos\frac{\beta_2}{2} + \sin\frac{\beta_2}{2}j,\\
l_z &= \cos\frac{\beta_3}{2} + \sin\frac{\beta_3}{2}k
\end{aligned}
\tag{21}
$$

and the quaternion for the composite rotation is $l = l_x\, l_y\, l_z$. If we let $g = l$, then β_1, β_2 and β_3 can be obtained. However further study suggests that these kinds of successive rotations are sequence-dependent, which means the YXZ-type rotations produce an orientation that is different from that of the XYZ-type rotations. This fact can also be seen by the non-commutativity of the quaternion (or rotation matrix), $l_x\, l_y\, l_z \neq l_y\, l_x\, l_z$ [16]. Consequently β_1, β_2 and β_3 determined using this method are not mutually independent, and thus not suitable for deciding the torques and forces between the two bonded particles.

Since the rotation g is unique, corresponding to the unique torques and forces, it is apparent that there must be a sequence-independent rotation serial corresponding to g. This idea is confirmed in the following part.

In fact the rotation g can be decomposed in a slightly different way. This rotation can always be decomposed into two rotations, the first is a rotation from $X_2'Y_2'Z_2'$ to a new frame $X'Y'Z'$, making the Z_2'-axis rotate over angle θ and coincide with the Z_1'-axis. The second rotation is from $X'Y'Z'$ to $X_1'Y_1'Z_1'$, which is an axial rotation of angle ψ about the $Z'(Z_1')$-axis (Fig. 8).

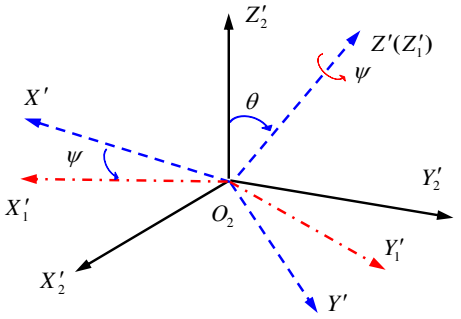

Fig. 8 The rotation from $X_2'Y_2'Z_2'$ to $X_1'Y_1'Z_1'$ can be decomposed into a rotation of angle θ from the Z_2'-axis to the Z_1'-axis, followed by an axial rotation of angle ψ about the Z_1'-axis

Since the quaternion $g = g_0 + g_1 i + g_2 j + g_3 k$ represents the rotation from $X_2'Y_2'Z_2'$ to $X_1'Y_1'Z_1'$, the unit vector of Z_1'-axis is (evaluated in $X_2'Y_2'Z_2'$)

$$
\begin{aligned}
\boldsymbol{o_2 z_1'} = g\hat{\boldsymbol{k}}g^{-1} &= 2(g_1 g_3 + g_0 g_2)\hat{\boldsymbol{i}} + 2(g_2 g_3 - g_0 g_1)\hat{\boldsymbol{j}}\\
&\quad + (g_0^2 - g_1^2 - g_2^2 + g_3^2)\hat{\boldsymbol{k}}
\end{aligned}
\tag{22}
$$

The axis and the angle of the first rotation (from $X_2'Y_2'Z_2'$ to $X'Y'Z'$) are vector $\boldsymbol{o_2 z_2'} \times \boldsymbol{o_2 z_1'} = 2(g_0 g_1 - g_2 g_3)\hat{\boldsymbol{i}} + 2(g_1 g_3 + g_0 g_2)\hat{\boldsymbol{j}}$ and θ, its quaternion can be determined as $m = m_0 + m_1 i + m_2 j + m_3 k$, where

$$
\begin{aligned}
m_0 &= \cos\frac{\theta}{2} = \sqrt{g_0^2 + g_3^2}, \quad m_1 = \frac{g_0 g_1 - g_2 g_3}{\sqrt{g_0^2 + g_3^2}},\\
m_2 &= \frac{g_1 g_3 + g_0 g_2}{\sqrt{g_0^2 + g_3^2}}, \quad m_3 = 0
\end{aligned}
\tag{23}
$$

The quaternion of the second rotation (from $X'Y'Z'$ to $X_1'Y_1'Z_1'$) is $n = \cos(\psi/2) + k\sin(\psi/2)$. If we let $mn = g$, the angle ψ is obtained from

$$
\cos\frac{\psi}{2} = \frac{g_0}{\sqrt{g_0^2 + g_3^2}}, \quad \sin\frac{\psi}{2} = \frac{g_3}{\sqrt{g_0^2 + g_3^2}}
\tag{24}
$$

From Eq. 22, the angle θ is determined by

$$
\cos\theta = g_0^2 - g_1^2 - g_2^2 + g_3^2
\tag{25}
$$

Next, we change the order of the two rotation sequences. The first one, from $X_2'Y_2'Z_2'$ to a new frame $X''Y''Z''$, is a rotation of angle ψ' about Z_2'-axis, with quaternion $n' = \cos(\psi'/2) + k\sin(\psi'/2)$.

The second rotation is from $X''Y''Z''$ to $X_1'Y_1'Z_1'$, making the $Z''(Z_2')$-axis rotate over angle θ and coincide with the Z_1'-axis (Fig. 9). Similarly, its quaternion (with respect to $X''Y''Z''$) is $m' = m'_0 + m'_1 i + m'_2 j + m'_3 k$, where

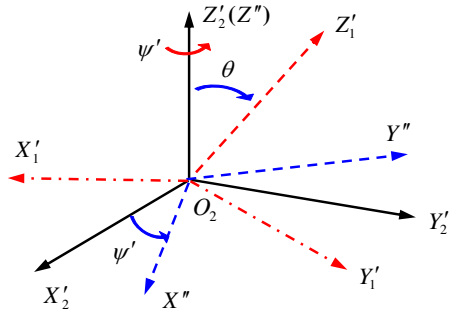

Fig. 9 Two rotations from $X_2'Y_2'Z_2'$ to $X_1'Y_1'Z_1'$ change order: an axial rotation of angle ψ about Z_2'-axis first, then followed by a rotation of angle θ from the Z_2'-axis to the Z_1'-axis

$$m_0' = \mathbf{cos}\frac{\theta}{2} = \sqrt{g_0^2 + g_3^2},$$
$$m_1' = \frac{(g_1g_3 + g_0g_2)\mathbf{sin}\psi' + (g_0g_1 - g_2g_3)\mathbf{cos}\psi'}{\sqrt{g_0^2 + g_3^2}},$$
$$m_2' = \frac{(g_1g_3 + g_0g_2)\mathbf{cos}\psi' - (g_0g_1 - g_2g_3)\mathbf{sin}\psi'}{\sqrt{g_0^2 + g_3^2}} \text{ and } m_3' = 0.$$

Let $n'm' = g$, we have $\mathbf{cos}\frac{\psi'}{2} = \frac{g_0}{\sqrt{g_0^2+g_3^2}}$ and $\mathbf{sin}\frac{\psi'}{2} = \frac{g_3}{\sqrt{g_0^2+g_3^2}}$.

The fact that $\psi' = \psi$ implies the two components of g are sequence-independent and therefore mutually independent.

Further study reveals that the rotation specified by the quaternion m (or m') can not be decomposed further into two independent rotations around the new $\boldsymbol{X}_2'$ and Y_2'-axis. If we assume so then we would have $vw = m$ or $wv = m$, where $v = \cos(\xi/2) + i\sin(\xi/2)$ and $w = \cos(\zeta/2) + j\sin(\zeta/2)$ are the quaternions for these two rotations, and ξ and ζ are assumed to be non-zero rotation angles. We note that $m_3 = 0$ in Eq. 23 requires $\sin(\xi/2)\sin(\zeta/2) = 0$, which implies either $\xi = 0$ or $\zeta = 0$, and hence the quaternion m can not be factorized into two independent rotations with non-zero angles.

Fortunately it is not necessary to further decompose the rotation m in the isotropic case, since this rotation can be viewed as "one" bending in a specified plane. The interactions caused by this bending can be uniquely computed if the bending angle θ and the orientation of that plane are known. The orientation of the plane is determined by the angle φ between the X_2'-axis and the $O_2\,Z_{xy}'$ (Fig. 4), where O_2Z_{xy}' is the projection of Z_1'-axis on the $X_2'Y_2'$ plane. From Eq. 22 and Fig. 4 φ can be determined using

$$\begin{aligned}\mathbf{cos}\varphi &= \frac{2(g_1g_3 + g_0g_2)}{\sqrt{4(g_1g_3 + g_0g_2)^2 + 4(g_2g_3 - g_0g_1)^2}} \\ &= \frac{g_1g_3 + g_0g_2}{\sqrt{(g_0^2 + g_3^2)(g_1^2 + g_2^2)}}, \\ \mathbf{sin}\varphi &= \frac{g_2g_3 - g_0g_1}{\sqrt{(g_0^2 + g_3^2)(g_1^2 + g_2^2)}}\end{aligned} \tag{26}$$

Similarly in the case corresponding to Fig. 9, it is found that the orientational angle φ' between X'-axis and O_2Z_{xy}' is $\varphi' = \varphi - \psi$ (O_2Z_{xy}' and φ' are not drawn in Fig. 9). This implied that in the case of Figs. 8 and 9, the bending of θ occurs exactly on the same plane (relative to O_2X_2') which is controlled by φ (or φ'). Therefore in addition to ψ and θ, φ (or φ') acts as the third parameter for g to be determined uniquely.

If we limit $0 \le \varphi \le 2\pi$, measured counterclockwise from the X_2'-axis, and $0 \le \theta \le \pi$, measured from the Z_2'-axis in radian, then ψ is determined by applying the right-hand rule around the Z_2' or Z_1'-axis. Then ψ, θ and φ can be decided uniquely by Eqs. 24–26.

We note that when $g_0 = \cos(\chi/2)$, $g_3 = \sin(\chi/2)$ and $g_1 = g_2 = 0$, we have $\theta = 0$ and $\psi = \chi$ (χ is a small angle). φ can not be decided since Eq. 26 is singular. In this case φ is redundant, because the rotation g_{21} corresponds to a pure twisting of χ around Z_2'-axis without bending. Another special case occurs when $g_0 = \cos(\chi/2)$, $g_2 = \sin(\chi/2)$, $g_1 = g_3 = 0$, which gives $\theta = \chi$, $\psi = 0$, $\varphi = 0$, and corresponds to bending of χ around Y_2'-axis without twisting.

In summary we have showed that an arbitrary rotation represented by g can not be decomposed into three mutually independent rotations specified in Eq. 21. Instead it can be decomposed into two rotations, one pure axial rotation of angle ψ around its Z_2'-axis, and one rotation of the Z_2'-axis over θ on a specified plane controlled by another parameter φ. These two rotations are sequence-independent and therefore mutually independent.

References

1. Allen MA, Tildesley DJ (1987) Computer simulation of liquid. Oxford Science, Oxford
2. Baranowski R,Thachuk M (1999) Mobilities of NO+ drifting in helium: a molecular dynamics study. J Chem Phys 110:11383–11389
3. Bauchau OA,Trainelli L (2003) The vectorial parameterization of rotation. Nonlinear Dyn 32:71–92
4. Buss SR (2000) Accurate and efficient simulation of rigid-body rotations. J Comp Phys 164:377–406
5. Coleman BD, Olson WK, Swigon D (2003) Theory of sequence-dependent DNA elasticity. J Chem Phys 115:7127–7140
6. Cundall PA,Stack ODL (1979) A discrete numerical model for granular assemblies. Geotechnique 29:47–65
7. Dullweber A, Leimkuhler AB, McLachlan R (1997) Symplectic splitting methods for rigid-body molecular dynamic. J Chem Phys 107:5840–5851
8. Evans DJ (1977) On the representation of orientation space. Mol Phys 34:317–325
9. Evans DJ, Murad S (1977) Singularity free algorithm for molecular dynamic simulation of rigid polyatomice. Mol Phys 34:327–331

10. Fincham D (1992) Leapfrog rotational algorithm. Mol Simul 8:165–178
11. Goldstein H (1990) Classical mechanics, 2nd edn. Addison-Wesley, Reading
12. Iwashita K, Oda M (1998) Rolling resistance at contacts in simulation of shear band development by DEM. J Eng Mech 124:285–292
13. Jiang MJ, Yu HS, Harris D (2005) A novel discrete element model for granular material incorporating rolling resistance. Comput Geotech 32:340–357
14. Johnson S, Willaims J, Cook B (2007) Quaternion-based approach for integration finite rotational motion. The proceedings of the 4th international conference on Discrete Element Method August, 2007, Brisbane, Australia, pp 27–29
15. Kol A, Laird BB, Leimkuhler BJ (1997) A symplectic method for rigid-body molecular simulation. J Chem Phys 107:2580–2588
16. Kuipers JB (1998) Quaternion and rotation sequences. Princeton University Press, Princeton
17. Miller III TF, Eleftheriou, Pattnaik MP,Vdirango,Newns AD (2002) Symplectic quaternion scheme for biophysical molecular dynamic. J Chem Phys 116:8649–8659
18. Mora P, Place D (1994) Simulation of the friction stick-slip instability. Pure Appl Geophys 143:61–87
19. Munjiza A, Latham JP, John NWM (2003) 3D dynamics of discrete element systems comprising irregular discrete elements-integration solution for finite rotations in 3D. Int J Numer Meth Eng 56:35–55
20. Omelyan IP (1998) Algorithm for numerical integration of the rigid-body equations of motion. Phys Rev E 58:1169–1172
21. Omelyan IP (1998) On the numerical integration of motion for rigid polyatomics: the modified quaternion approach. J Comp Phys 12:97–103
22. Omelyan IP (1998) Numerical integration of the equation of motion for rigid polyatomics: the matrix method. Comput Phys Commun 109:171–183
23. Place D, Mora P (1999) The lattice solid model to simulate the physics of rocks and earthquakes: incorporation of friction. J Comp Phys 150:332–372
24. Potyondy D, Cundall P (2004) A bonded-particle model for rock. Int J Rock Mech Min Sci 41:1329–1364
25. Rapaport DC (1995) The art of molecular dynamic simulation. Cambridge University press, Cambridge
26. Wang YC, Abe S, Latham S, Mora P (2006) Implementation of particle-scale rotation in the 3-D lattice solid model. Pure Appl Geophys 163:1769–1785
27. Wang YC, Mora P (2008) Modeling wing crack extension: implications to the ingredients of discrete element model. Pure Appl Geophys (in print)